Magazine of Concrete Research, 2006, **58**, No. 10, December, 647–656

Constitutive behaviour of high-performance ferrocement under axial compression

P. Rathish Kumar* and C. B. K. Rao*

National Institute of Technology, Warangal, India

The increased utility of ferrocement for stressed skin surfaces such as domes, arches, funicular shells etc, necessitated further research and development for better performance. The aim of the current paper is to develop an analytical model for predicting the stress–strain behaviour of an improved ferrocement, based on the experimental results. The results of 144 hollow cylindrical specimens tested under strain control rate of loading are presented. The increase in strength and strain of ferrocement are used in formulating the constitutive relation.

Introduction

The structural behaviour of ferrocement is different from conventional reinforced concrete. The dispersion of small-diameter steel wires closely and uniformly spaced in the entire volume of the cement mortar improves many engineering properties such as impact and fatigue resistance, tensile strength, toughness and flexural strength.[1–5] Essentially, the mesh reinforcement acts as crack arrestors, resisting the development of crack.[6,7] The use of normal-strength mortars in ferrocement limits the beneficial effect of closer spacing of the reinforcement. The dispersion of the mesh in normal mortar matrices exhibits the susceptibility for permeability and corrosion attack. Therefore, even though it was demonstrated that ferrocement is a material with good performance, there is a need to plug the deficiencies to make it truly versatile in all aspects, particularly regarding performance aspects related to permeability and corrosion.[8,9] The inhibition depends on the impermeability of the mortar phase. Hence, it is necessary to introduce performance mortars in place of normal mortars in ferrocement.[10] Such a material can be termed 'high-performance ferrocement' (HPF). The ferrocement model code[11] and work by Naaman[12] also demonstrated the need for use of high-strength and durable mortars for use in ferrocement works. The use of HPF is believed to further improve the market penetration of ferrocement and its acceptance. The construction of ferrocement shells has been found attractive in many developing countries because of advantages such as availability of the basic raw materials and easy fabrication of ferrocement into any shape and economy. Further, the skills required for the construction of ferrocement can be easily acquired and are less capital intensive and more labour intensive.

The main parameters of the present study are the diameter of wire and spacing of wires in the mesh, the number of layers of mesh, the yield strength of the mesh wire and the strength of mortar. A single non-dimensional parameter called 'specific surface factor' (S_F)[7] is identified by involving all the parameters that influence the behaviour of ferrocement. The specific surface ratio (s) is the ratio of the total surface area of contact of reinforcement wires present in the unit length in the direction of application of load and in a given width and thickness of the specimen to the volume of the mortar per unit length of the specimen in the direction of loading with the same width and thickness. The specific surface ratio, the yield stress of wires and the plain mortar strength were combined to obtain the specific surface factor

$$S_F = s.\sigma_y/\sigma_p \quad (1)$$

$$\text{The specific surface ratio } s = \frac{\pi d \times n \times N \times 1}{b \times h \times 1} \quad (2)$$

where d is the diameter of wire, n is the number of wires in one layer, N is the number of layers of wire mesh and b and d represent the mean diameter and the thickness of the specimen.

* National Institute of Technology, Warangal 506 004, Andhra Pradesh, India

(MCR 51468) Paper received 7 October 2005; accepted 13 March 2006

www.concrete-research.com 1751-763X (Online) 0024-9831 (Print)

Research significance

Ferrocement can be effectively used in the construction of single or double curved shells and folded plates. These elements are subjected to compressive stresses in certain zones. Although the individual parameters that affect the behaviour of ferrocement in compression have been identified, very little work is available to establish quantitatively the ultimate strength, strain at ultimate strength and the modulus of elasticity of ferrocement specimens for a given set of parameters. Further, with the exception of the work by Nedwell and Nakassa[13] who have reported results of HPF under flexural load, there is no other work reported in literature on HPF in axial compression. The present investigation hence aims at developing the stress–strain curve in axial compression of an improved ferrocement. A relation is proposed for the constitutive behaviour of HPF under axial compression.

Experimental programme

The experimental programme consisted of casting and testing 144 hollow cylindrical specimens of 150 mm external diameter, 20 mm thickness and 150 mm height. The hollow cylindrical specimens have the advantage of stability and facilitated axial loading without much difficulty.

High-performance mortars

The specimens were cast with high-performance mortars developed by the current authors, the details of which are reported elsewhere.[14–18] The authors have tested different types of cements, mixes and used various mineral and chemical admixtures. In the present investigation the specimens were cast in three groups. The first group of specimens was cast with mortar mix X (cement to sand 1:1/0·34 water/cement (w/c) ratio), the second with mortar mix Y (1:1·5/0·36 w/c ratio) and the third mix Z (1:2/0·38 w/c ratio). Slag cement with a specific gravity 3·161, sand passing through a 1·2 mm sieve with a fineness modulus of 2·4 and a specific gravity of 2·44, optimum dosage of 10% of silica fume by weight of cement were used. The silica fume had silica content of 92% and was obtained as a by-product from a Ferro silicon industry. Silica fume was used as a partial replacement for slag cement. Workability reduced when fine silica fume was added to cement. Hence, this problem was fixed by using a water-reducing admixture. The cube strength and flow properties of the high-performance mortar used for casting the specimens are shown in Table 1.

The drying shrinkage was obtained using standard-length comparator and the strains obtained are shown in Fig. 1. The combined effect of optimum dosages of silica fume and superplasticiser has resulted in lower shrinkage strains[15] not exceeding 300×10^{-6}. None of the three mixes exceeded this shrinkage strain.[19]

Table 1. Properties of cement mortars

S No.	Mix	Flow	Compressive strength: MPa		
			3 days	7 days	28 days
1	1:1/0·34	116	38	57	81
2	1:1·15/0·35	128	32	43	70
3	1:1·2/0·37	130	28	38	62

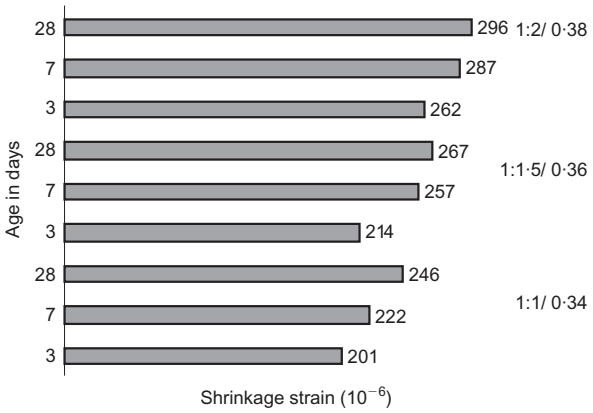

Fig. 1. Age plotted against shrinkage strain

Sorptivity is an indirect measure of measuring the permeability. It is defined as the tendency of a porous material to absorb and transmit water by capillarity.[20] Specimens of size 100×100 mm were used for sorptivity tests. The sorptivity was determined measuring the capillary rise absorption rate on reasonably homogenous materials. Water was used as the test fluid. The sample was rested on rods or pins to allow free access of water to the inflow surface. The water level was kept not more than 5 mm above the base of the specimen. The quantity of water absorbed in a time period of 30 min was measured by weighing the specimen. The schematic diagram of the test set-up is shown in Fig. 2.

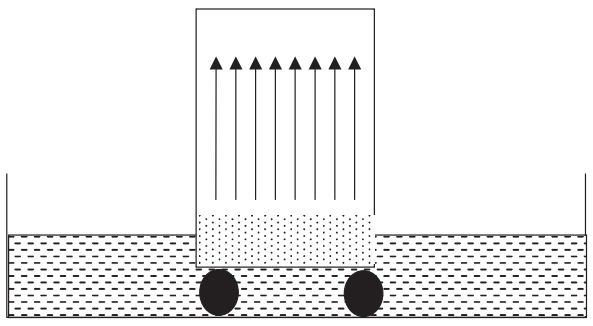

Fig. 2. Sorptivity test set-up

The sorptivity is given by $i/\sqrt{t}$, where $i = \Delta w/Ad$ and t is the soaked time in minutes, Δw is the increase in weight of the specimen, A is the surface area of the specimen through which the water penetrated and d is the density of the fluid medium (water). Fig. 3 shows the plot for the variation of sorptivity with age for different mixes. The water sorptivity decreased with increase in age of mortars for all the mixes.

In general it may be noted that high-performance mortars developed using slag cement with optimum dosages of silica fume and superplasticiser provided good flowability and strength. The shrinkage strains and sorptivity values of the three mortar mixes were very much appreciable. The mortars were dense and impermeable. Use of these mortars in ferrocement resulted in an improved performance of ferrocement.[8]

Preparation of the ferrocement specimens

Each of the three groups of hollow cylindrical specimens designated X, Y and Z as per the type of mix, were cast in four batches (A, B, C, D representing the four types of meshes). The specimens in each batch were divided into four sets (plain, four layers, five layers and six layers). In each set three identical specimens were cast and tested and the average behaviour was taken to represent the behaviour for that set of three specimens. The details of the properties of the mesh wire and the strength of the plain hollow cylindrical specimens are shown in Table 2.

In each batch the total number of hollow cylindrical specimens was 12 including the plain mortar and four-, five- and six-layered ferrocement specimens for a particular mix. Square woven galvanised wire mesh of required size 145 mm wide and of length slightly more than that required to obtain the number of layers was cut from the standard mesh roll. The 145 mm length transverse wires formed the wires in the vertical direction, that is, the vertical axis of the specimen. The mesh was wound tightly to conform to the cylindrical shape of the specimen. The details of the fabrication of the mesh are shown in Fig. 4.

The standard 150 mm diameter and 300 mm cast iron cylindrical mould was fitted with a solid 150 mm height teak wood cylinder at the bottom. One more wooden cylinder of diameter equal to the inner diameter of the ferrocement hollow cylindrical specimen and height equal to 50 mm more than the height of the specimen was placed in the central recess of the bottom cylinder to obtain the required uniform thick annular space over a height of 150 mm. A typical mould for casting the specimens is shown in Fig. 5.

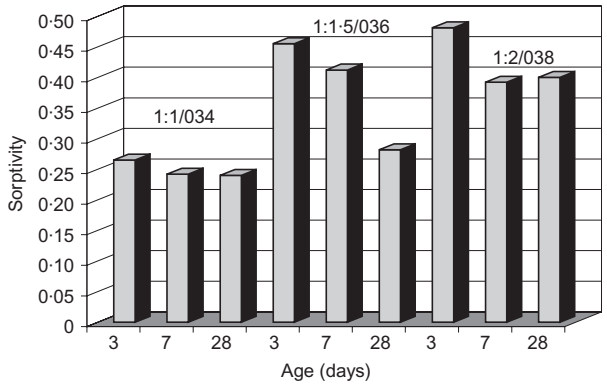

Fig. 3. Age plotted against sorptivity

The fabricated mesh (Fig. 6) was placed in the annular space of the mould. Spacer rods were kept in between the mesh layers and cover pieces were provided on the inner and outer surfaces. The mortar was filled in between the mesh layers, simultaneously vibrating the moulds. After about 4 h of casting, the specimens were cured with damp burlap to prevent moisture loss. The specimens were stripped off the moulds 28 days after casting and then air cured before testing. Companion plain mortar hollow cylindrical specimens were cast to obtain direct compression strength.

Test set-up

The cured specimens were capped with plaster of Paris before testing, to provide a smooth loading surface. The Tinius–Olsen testing machine of 1810 kN was used for testing the hollow cylindrical specimens under uniaxial compression. It was observed that the resistance strain gauges and demec points fixed to the specimen surface became separated owing to the spalling of the mortar under them. Hence, a set-up similar to the compressometer designed to measure the strains in concrete cylinders was used. Each frame was attached to the specimen by screws that were positioned at the mid-points of the sides of the frame. The two frames were attached to vertical aluminium plates that were fixed to the top frame. The two frames were attached to the specimen symmetrically at the required gauge length, that is, 100 mm apart. Dial gauges with least count of 0·001 mm were attached to vertical aluminium plates fixed to the top frame. The movable spindles of the dial gauges rested on the plane circular heads of the adjustable screws, which were positioned in mild steel plates projecting horizontally from the bottom frame. The frames were attached to the specimen by means of screws, which would fit snugly to the specimen. Fig. 7 shows the details of the compressometer attached to the specimen.

Experimental stress–strain curves

From the observed data, for a given specimen, the longitudinal deformations were calculated from the average readings of the four dial gauges of the compressometer. The stress–strain curves were drawn for three companion specimens of a set with the same

Table 2. Properties of mesh wires and mortar

S No.	Designation	Plain mortar strength: MPa	Reinforcement in the direction of force			S_F
			Diameter: mm	No. of wires in C/S	Yield strength: MPa	
1	AX4	58·5	0·47	440	575·0	7·818
2	AX5	58·5	0·47	550	575·0	9·770
3	AX6	58·5	0·47	660	575·0	11·726
4	BX4	58·0	0·37	552	472·0	6·396
5	BX5	58·0	0·37	690	472·0	7·990
6	BX6	58·0	0·37	828	472·0	9·600
7	CX4	58·5	0·47	584	512·5	9·250
8	CX5	58·5	0·47	730	512·5	11·560
9	CX6	58·5	0·47	876	512·5	13·870
10	DX4	59·2	0·57	340	350·0	4·419
11	DX5	59·2	0·57	425	350·0	5·530
12	DX6	59·2	0·57	510	350·0	6·630
13	AY4	50·5	0·47	440	575·0	8·700
14	AY5	50·5	0·47	550	575·0	10·80
15	AY6	50·5	0·47	660	575·0	13·06
16	BY4	54·0	0·37	552	472·0	6·870
17	BY5	54·0	0·37	690	472·0	8·583
18	BY6	54·0	0·37	828	472·0	10·314
19	CY4	53·0	0·47	584	512·5	10·211
20	CY5	53·0	0·47	730	512·5	12·764
21	CY6	53·0	0·47	876	512·5	15·317
22	DY4	53·0	0·57	340	350·0	4·900
23	DY5	53·0	0·57	425	350·0	6·150
24	DY6	53·0	0·57	510	350·0	7·380
25	AZ4	49·5	0·47	440	575·0	9·240
26	AZ5	49·5	0·47	550	575·0	11·540
27	AZ6	49·5	0·47	660	575·0	13·850
28	BZ4	44·0	0·37	552	472·0	8·430
29	BZ5	44·0	0·37	690	472·0	10·530
30	BZ6	44·0	0·37	828	472·0	12·660
31	CZ4	55·0	0·47	584	512·5	12·027
32	CZ5	55·0	0·47	730	512·5	15·030
33	CZ6	55·0	0·47	876	512·5	18·040
34	DZ4	47·5	0·57	340	350·0	5·550
35	DZ5	47·5	0·57	425	350·0	6·867
36	DZ6	47·5	0·57	510	350·0	8·238

origin and the average curve was taken to represent the set. Such average curves for all the sets of a typical batch with a common origin are shown in Fig. 8.

Behaviour of specimens under loading

All the specimens were tested under a strain rate control of 670 μ mm/mm per min. The load increased rapidly in the initial steps up to 75% of ultimate load and increased at a slower rate until the ultimate load was reached. Tests were continued until the load dropped by 70–75% of the ultimate load. Beyond the ultimate load the strains increased at a rapid rate and were accompanied by a decrease in the load-carrying capacity of the specimen. The higher the specific surface factor, the lower was the rate of decrease of load. The maximum stress and the strain at ultimate load increased with the specific surface factor. Vertical cracks distributed around the specimen were noticed on the specimen with increase in the load. The cracks progressed from the bottom to the top with further increase of load. The extent of cracking and the rate of decrease of load after the peak (in the descending portion of the stress–strain curve) depended upon the specific surface factor (S_F) of the ferrocement for all the mixes. The higher the S_F, the lower is the rate of decrease of load and extent of spalling. This may be attributed to the improvement in the internal crack-arresting mechanism, dimensional stability as well as the integrity of the material caused by the presence of large volume fraction of the mesh reinforcement present in the mortar matrix. Also, the presence of the mesh resulted in an improved strength and ductility of HPF. The results of ultimate strength, strain at ultimate strength and the modulus of elasticity of ferrocement specimens as a ratio with respect to identical plain mortar specimens are shown in Table 3. A comparison of the different values indicates that when the same mesh is used, there is an increase in the strength and

(a) Inner layer

(b) Outer layer

Fig. 4. Fabrication of the mesh layers

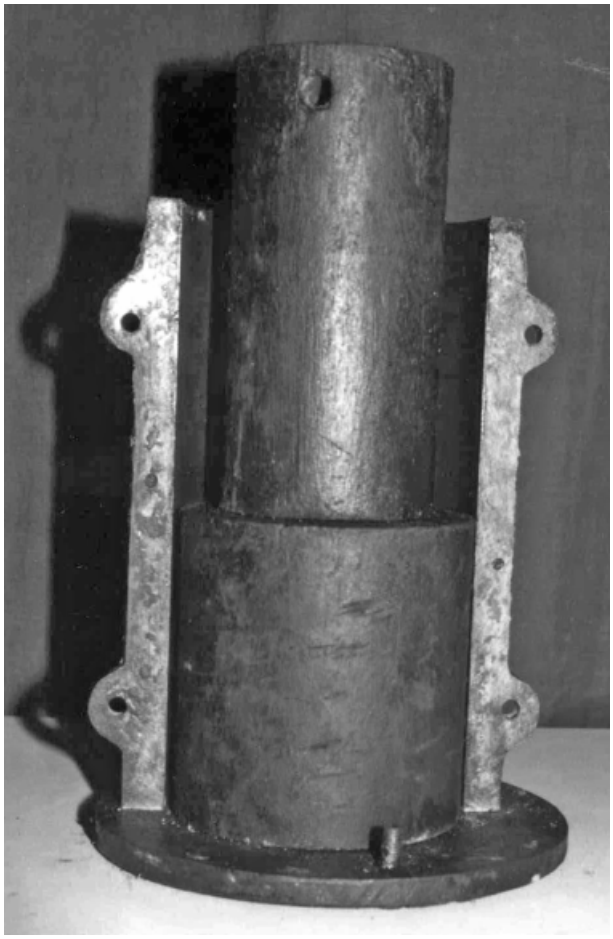

Fig. 5. Typical mould

strain values with increasing number of layers of the mesh. The mesh with smaller diameter wires having smaller openings with all the other variables remaining the same, resulted in marginally increased values of the ultimate strength, strain at ultimate strength and modulus of elasticity because of the higher specific surface area. The ultimate strength of HPF, strain at ultimate strength and the modulus of elasticity varied linearly with the specific surface factor (S_F) of the ferrocement. The prediction equations fit for the same are

$$\sigma_c/\sigma_p = 1{\cdot}0 + 0{\cdot}010S_F \quad (3)$$

$$\varepsilon_c/\varepsilon_p = 1{\cdot}0 + 0{\cdot}032S_F \quad (4)$$

$$E/E_P = 1{\cdot}05 + 0{\cdot}022S_F \quad (5)$$

The variations of the stress ratio (σ_c/σ_p), strain ratio ($\varepsilon_c/\varepsilon_p$) and the modular ratio (E/E_P) with respect to the specific surface factor are shown in Figs 9 to 11 respectively.

Non-dimensionalised stress–strain curve

An examination of the curves in Fig. 8 indicates that the behaviour is similar for all the specimens; that is the stress–strain behaviour is linear up to 80–90% of the ultimate and non-linear beyond this. The post-peak

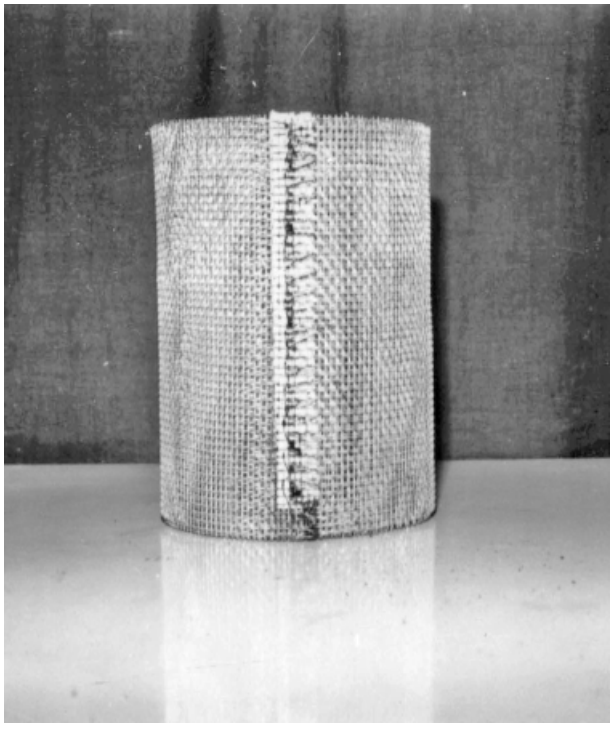

Fig. 6. Fabricated mesh

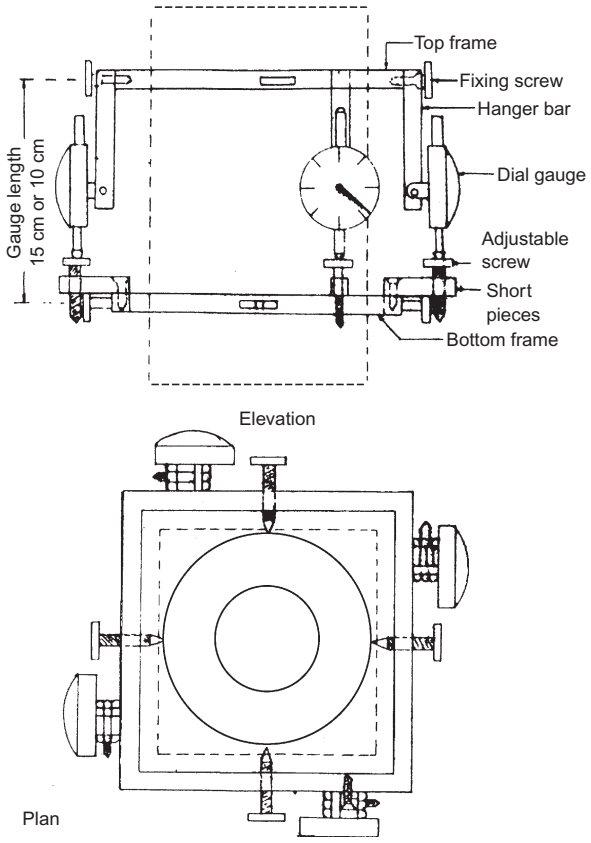

Fig. 7. Details of the set-up of the compressometer

stress–strain response for all the ferrocement specimens is gradual and appears to have a consistent and constant gradient; particularly for a given mesh and mortar strength the curves are almost parallel for four, five and six layers. This similarity leads to the conclusion that if the stress is expressed as a stress ratio by dividing the stress at any level by the corresponding ultimate strength of that specimen and the strains are expressed as strain ratio, by dividing the strain at any level by the corresponding strain at ultimate strength, the plot of these two ratios falls into the same pattern. By non-dimensionalising the stress and strain as above, the influence of the ferrocement parameters is eliminated for each specimen. Fig. 12 shows the values of the non-dimensionalised stress (stress ratio) and non-dimensionalised strain ratio as abscissa. Fig. 13 shows the values along with the mean, minimum, maximum and the characteristic values. The plots indicate that the stress–strain behaviour of HPF can be represented by a general curve, which functions as a stress block. A single polynomial, similar in form to that originally proposed by Sargin *et al.*[21] for concrete is used in the current investigation.

The model is of the form

$$\sigma = \frac{A\varepsilon + D\varepsilon^2}{1{\cdot}0 + B\varepsilon + C\varepsilon^2} \tag{6}$$

where σ is the stress at any level and ε is the strain at any level.

To express the non-dimensional stress–strain curves the following form is proposed

$$\frac{\sigma}{\sigma_c} = \frac{A'(\varepsilon/\varepsilon_c) + D'(\varepsilon/\varepsilon_c)^2}{1 + B'(\varepsilon/\varepsilon_c) + C'(\varepsilon/\varepsilon_c)^2} \tag{7}$$

where σ_c and ε_c are the ultimate stress and ultimate strain of the ferrocement specimen in compression. A single equation to predict the complete behaviour has been obtained using the following boundary conditions

(*a*) $@\frac{\varepsilon}{\varepsilon_c} = 1; \frac{\sigma}{\sigma_c} = 1$

(*b*) $@\frac{\varepsilon}{\varepsilon_c} = 1; \frac{d(\sigma/\sigma_c)}{d(\varepsilon/\varepsilon_c)} = 0$

(*c*) $@\frac{\varepsilon}{\varepsilon_c} = 2{\cdot}8; \frac{\sigma}{\sigma_c} = 0{\cdot}875$ (descending portion)

(*d*) $@\frac{\varepsilon}{\varepsilon_c} = 0{\cdot}6; \frac{\sigma}{\sigma_c} = 0{\cdot}87$ (ascending portion)

The conditions (*c*) and (*d*) are obtained from the experimental data. The constants *A*, *B*, *C* and *D* satisfying the above conditions are 0·051, −1·949, 3·875 and 2·875. Thus the stress–strain equation for HPF in direct compression is

$$\frac{\sigma}{\sigma_c} = \frac{0{\cdot}051(\varepsilon/\varepsilon_c) + 2{\cdot}875(\varepsilon/\varepsilon_c)^2}{1 - 1{\cdot}949(\varepsilon/\varepsilon_c) + 3{\cdot}875(\varepsilon/\varepsilon_c)^2} \tag{8}$$

Hence the generalised stress–strain equation for HPF can be written as

$$\sigma = \frac{A\varepsilon + D\varepsilon^2}{1{\cdot}0 + B\varepsilon + C\varepsilon^2}$$

where

$$A = A'\left(\frac{\sigma_c}{\varepsilon_c}\right) = 0{\cdot}051\left(\frac{\sigma_c}{\varepsilon_c}\right)$$

$$B = B'\left(\frac{1}{\varepsilon_c}\right) = -1{\cdot}949\left(\frac{1}{\varepsilon_c}\right)$$

$$C = C'\left(\frac{1}{\varepsilon_c^2}\right) = 3{\cdot}875\left(\frac{1}{\varepsilon_c^2}\right)$$

$$D = D'\left(\frac{\sigma_c}{\varepsilon_c^2}\right) = 2{\cdot}875\left(\frac{f_c}{\varepsilon_c^2}\right)$$

The non-dimensionalised stress–strain curve using the above constants is shown in Fig. 14. The proposed theoretical curve is very close to the experimental point, with a coefficient of correlation of 0·986. The stress block parameters that are useful in computing the ultimate moment of resistance and corresponding curvature of HPF section may hence be obtained using the above-proposed stress–strain equation.

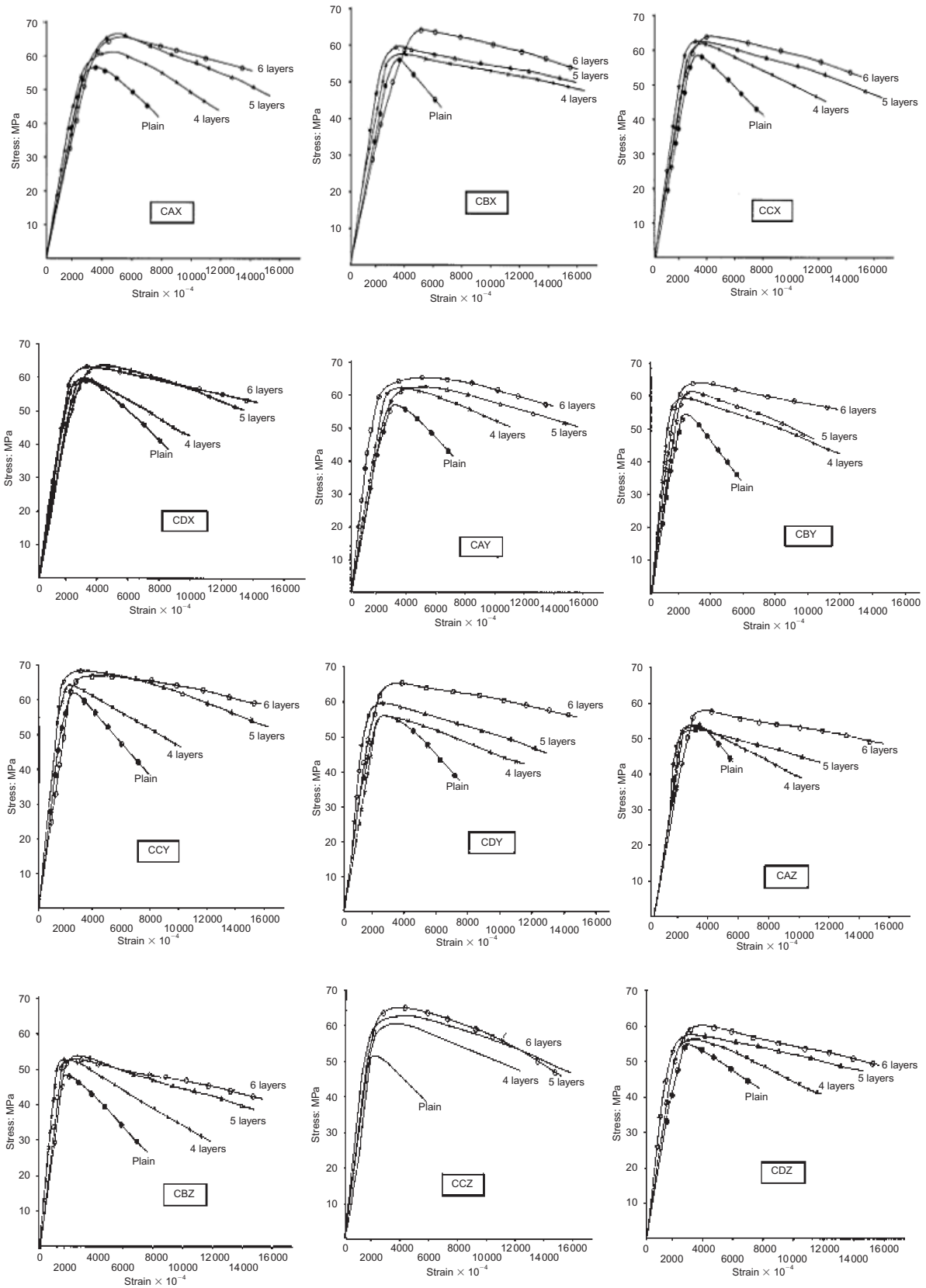

Fig. 8. Stress–strain diagrams

Conclusions

The following conclusions can be drawn from the experimental investigation on HPF.

(*a*) The mortars developed with optimum dosages of silica fume and superplasticiser using slag cement resulted in good strength and durable mortars. The mortars were dense, impermeable and had good

Table 3. Test results of HPF specimens

Designation	Stress ratio σ_u/σ_p	Strain ratio $\varepsilon_u/\varepsilon_p$	Modular ratio E/E_P	Designation	Stress ratio σ_u/σ_p	Strain ratio $\varepsilon_u/\varepsilon_p$	Modular ratio E/E_P	Designation	Stress ratio σ_u/σ_p	Strain ratio $\varepsilon_u/\varepsilon_p$	Modular ratio E/E_P
AX4	1·077	1·364	1·060	AY4	1·095	1·036	0·974	AZ4	0·980	1·090	1·000
AX5	1·162	1·450	1·115	AY5	1·158	1·786	1·155	AZ5	0·990	1·130	1·250
AX6	1·171	1·545	1·252	AY6	1·162	1·857	1·720	AZ6	1·081	1·390	1·335
BX4	1·017	0·955	0·867	BY4	1·093	0·957	1·110	BZ4	1·091	0·947	1·000
BX5	1·069	1·045	1·131	BY5	1·130	1·217	1·250	BZ5	1·091	1·053	1·011
BX6	1·138	1·490	1·250	BY6	1·176	1·304	1·330	BZ6	1·125	1·316	1·455
CX4	1·060	0·937	1·124	CY4	1·038	0·909	1·000	CZ4	1·167	1·556	1·112
CX5	1·068	1·209	1·124	CY5	1·085	1·273	1·250	CZ5	1·178	1·770	1·252
CX6	1·085	1·280	1·264	CY6	1·104	1·909	1·250	CZ6	1·267	1·830	1·428
DX4	1·017	1·000	0·987	DY4	1·000	0·880	1·200	DZ4	1·011	1·000	1·252
DX5	1·068	1·067	1·111	DY5	1·066	1·000	1·428	DZ5	1·042	1·270	1·409
DX6	1·085	1·400	1·212	DY6	1·17	1·240	1·500	DZ6	1·084	1·500	1·608

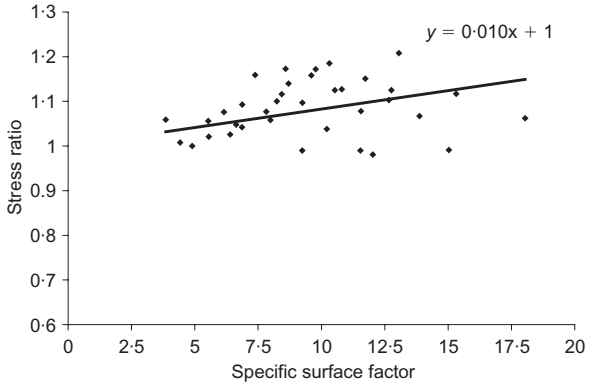

Fig. 9. Specific surface factor plotted against stress ratio

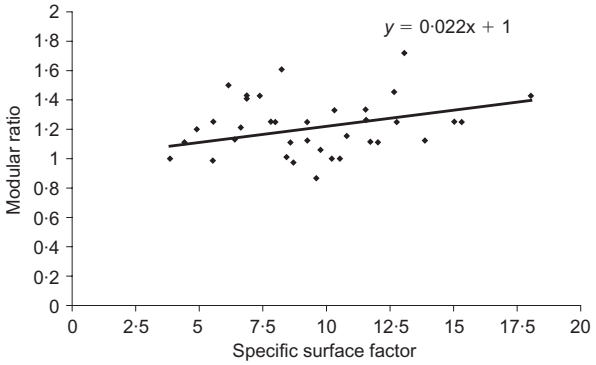

Fig. 11. Specific surface factor plotted against modular ratio

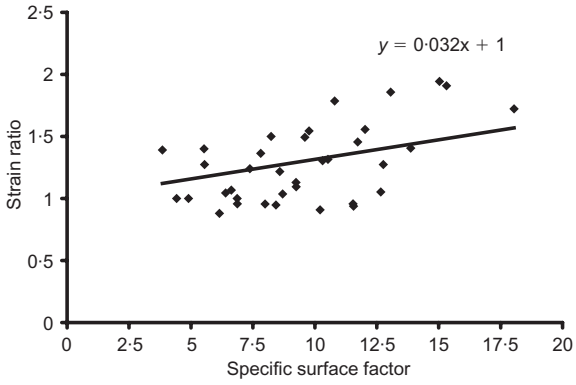

Fig. 10. Specific surface factor plotted against strain ratio

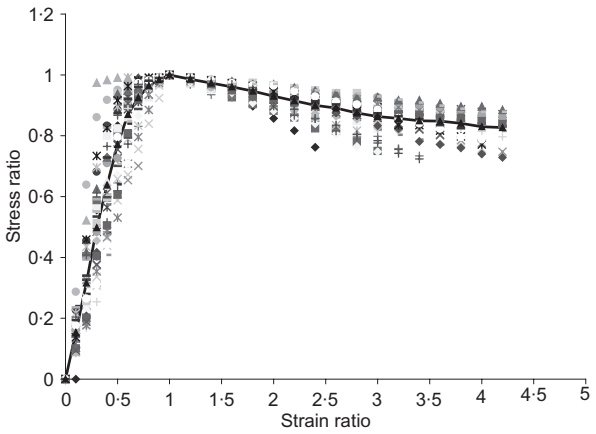

Fig. 12. Experimental stress ratio plotted against strain ratio; the symbols represent average points of several specimens

flowability, which is important for ferrocement works.

(*b*) The improvement in the performance of mortars in ferrocement has the advantage over normal mortars in improving the material properties such as integrity, dimensional stability and performance under large deformations.

(*c*) The stress–strain behaviour of HPF was linear up to 80–90% of the ultimate strength in axial compression and beyond this limit the behaviour became non-linear.

(*d*) The ultimate compressive strength varied linearly

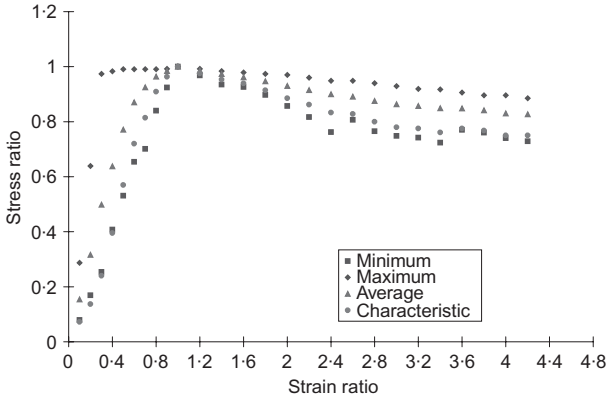

Fig. 13. Statistical values of the experimental points

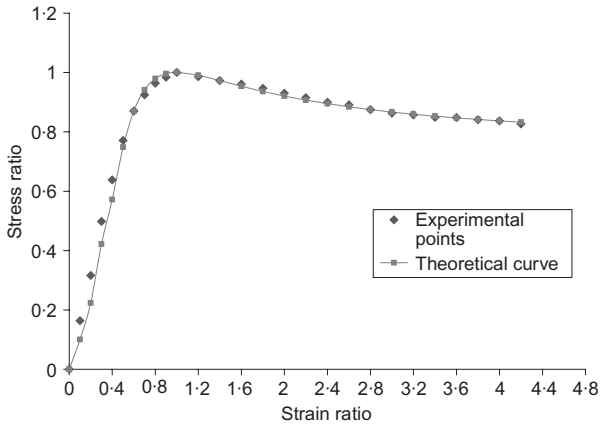

Fig. 14. Non-dimensionalised stress–strain curve

with the increase in the number of layers and can be expressed by a relationship including the specific surface factor. The prediction equation for ultimate strength is $\sigma_c/\sigma_p = 1{\cdot}0 + 0{\cdot}010\ S_F$.

(*e*) The strain at peak stress varies linearly with the specific surface factor and can be expressed by a relationship including specific surface factor. The equation obtained by regression analysis is $\varepsilon_c/\varepsilon_p = 1{\cdot}0 + 0{\cdot}032\ S_F$.

(*f*) The modular ratio defined as the ratio of secant modulus of elasticity for ferrocement to the modulus of elasticity of plain mortar varies linearly with specific surface factor. The regression analysis equation is given by $E/E_P = 1{\cdot}05 + 0{\cdot}022\ S_F$.

(*g*) The non-dimensional characteristic equation proposed in this investigation can be used to predict the constitutive behaviour of HPF in axial compression with reasonable accuracy.

(*h*) HPF specimens undergo large strains beyond the ultimate load without considerable decline of stress. This behaviour reveals a large energy absorption capacity of HPF.

Acknowledgement

The authors wish to thank the Director of the National Institute of Technology, Warangal, India for providing the necessary infrastructure in carrying out this research work.

References

1. Pama R. P., Robles A. L. R and Rubio-Hermosura N. Current researches on ferrocement. *Journal of Ferrocement*, 1993, **23**, No. 4, 227–288.
2. Walliuidin A. M. and Rafeeqi S. F. A. Study of behaviour of plain concrete confined with ferrocement. *Journal of Ferrocement*, 1994, **24**, No. 2, 139–145.
3. Balaguru P. Use of ferrocement for confinement of concrete. *Proceedings of the Third International Conference on Ferrocement,* Roorkee, India, 1988, pp. 296–305.
4. Rathish Kumar P. *Improvement in Ductility of High Strength Concrete with Ferrocement Shell in Addition to Rectangular Ties*. Master's thesis, Department of Civil Engineering, Regional Engineering College, Warangal, 1992.
5. American Concrete Institute. Guide for the design, construction and repair of ferrocement. *ACI Structural Journal*, 1988, **85**, No. 3, 325–351. ACI Committee 5491-R88.
6. Kumar G. R. Behaviour of high strength concrete confined with ferrocement shell in addition to lateral ties. *Journal of Ferrocement*, 2001, **31**, No. 3, 213–222.
7. Rathish Kumar P. Ferrocement: an effective way of confining high strength concrete. *Journal of Indian Association of IABSE*, 2002, **32,** No. 3, 17–28.
8. Rathish Kumar P. *A Study on Ferrocement with High Performance Mortar (FHPM) in Biaxial States of Stress*. PhD thesis, Department of Civil Engineering, National Institute of Technology, Warangal, 2003.
9. Rathish Kumar P. Ferrocement: the composite material of the future. *45th Congress of the Indian Society of Theoretical and Applied Mathematics, December 26–29, 2000*. Indian Institute of Technology, Kharagpur, India, 2000, pp. 137–138.
10. Rathish Kumar P. and Rao C. B. K. A study on the effect of silica fume and superplasticizer in rich mortar mixes. In *Proceedings of the National Conference on Materials and Structures*. National Institute of Technology, Warangal, India, 2004, pp. 131–136
11. International Foundation for Science. *Building Code Recommendations for Ferrocement (IFS 10–01), Ferrocement Model Code*. IFIC AIT Bangkok, 2001. IFS Committee 10.
12. Naaman A. E. *Ferrocement and Laminated Cementitious Composites*. Techno Press 3000, Michigan, 2000.
13. Nedwell P. J. and Nakassa A. S. High performance ferrocement using stainless steel mesh and high strength mortar. *Journal of Ferrocement*, 1999, **29**, No. 3, 189–194.
14. Rathish Kumar P., Seshu D. R. and Rao C. B. K. Studies on high performance mortar mixes: part 1 strength and flow characteristics. *International Journal of Ferrocement*, 2002, **32**, No. 3, 205–214.
15. Rathish Kumar P., Seshu D. R. and Rao C. B. K. Studies on high performance mortar mixes: part 2 shrinkage and sorptivity characteristics. *International Journal of Ferrocement*, 2002, **32**, No. 3, 215–231.
16. Rathish Kumar P., Manoj Kumar P., Rajsekhar P. and Nageswar G. A study on the sorptivity characteristics of high performance mortars. *Journal of Institution of Engineers (India)*, 2002, **83**, No. 1, 1–7.

17. Rathish Kumar P., Seshu D. R. and Sudhakar M. Effect of water cementitious ratio on the compressive strength of silica fume concrete. *Journal of Indian Concrete Institute*, 2001, **2**, No. 4, 37–40.
18. Rathish Kumar P. Superplasticizers in high strength mortars for use on ferrocement works. In *26th International Conference on Our World in Concrete and Structures, 27–28 August, 2001* (Tan J. S. Y. (ed.)). CI-Premier Pte. Ltd, Singapore, 2001, pp. 188–194.
19. Neville A. M. *Properties of Concrete*, 5th edn. Pearson Education, London, 2005.
20. Hall C. Water sorptivity of mortars and concretes: a review. *Magazine of Concrete Research*, 1989, **41**, No. 147, 51–61.
21. Sargin M., Ghosh S. K. and Handa V. K. Effects of lateral reinforcement upon the strength and deformations properties of concrete. *Magazine of Concrete Research*, 1971, **23**, Nos 75–76, 99–110.

Discussion contributions on this paper should reach the editor by 1 June 2007